Journal of Physiology (1995), **488.3**, *pp.*633–645

Kinetic characterization of rat brain type IIA sodium channel α-subunit stably expressed in a somatic cell line

Saumendra N. Sarkar, Arunabha Adhikari and S. K. Sikdar*

Molecular Biophysics Unit, Indian Institute of Science, Bangalore 560012, India

1. The rat brain type IIA Na^+ channel α-subunit was stably expressed in Chinese hamster ovary (CHO) cells. Current through the expressed Na^+ channels was studied using the whole-cell configuration of the patch clamp technique. The transient Na^+ current was sensitive to TTX and showed a bell-shaped peak current *vs.* membrane potential relation.

2. Na^+ current inactivation was better described by the sum of two exponentials in the potential range −30 to +40 mV, with a dominating fast component and a small slower component.

3. The steady-state inactivation, h_∞, was related to potential by a Boltzmann distribution, underlying three states of the inactivation gate.

4. Recovery of the channels from inactivation at different potentials in the range −70 to −120 mV were characterized by an initial delay which decreased with hyperpolarization. The time course was well fitted by the sum of two exponentials. In this case the slower exponential was the major component, and both time constants decreased with hyperpolarization.

5. For a working description of the Na^+ channel inactivation in this preparation, with a minimal deviation from the Hodgkin–Huxley model, a three-state scheme of the form $O \rightleftharpoons I_1 \rightleftharpoons I_2$ was proposed, replacing the original two-state scheme of the Hodgkin–Huxley model, and the rate constants are reported.

6. The instantaneous current–voltage relationship showed marked deviation from linearity and was satisfactorily fitted by the constant-field equation.

7. The time course of activation was described by an m^x model. However, the best-fitted value of x varied with the membrane potential and had a mean value of 2.

8. Effective gating charge was determined to be $4{\cdot}7e$ from the slope of the activation plot, plotted on a logarithmic scale.

9. The rate constants of activation, α_m and β_m, were determined. Their functional dependence on the membrane potential was investigated.

Neuronal excitability is mediated by ion-specific channel proteins through which membrane currents flow. The rising phase of the action potential is caused by an influx of Na^+ ions through voltage-activated Na^+ channels (Hille, 1992). The mammalian brain Na^+ channel is a heterotrimeric protein consisting of a large glycosylated α-subunit of 230–270 kDa and two smaller β1- and β2-subunits (36 and 33 kDa, respectively). Different cDNA clones encoding highly homologous subtypes (types I, II, IIA, and III) of the α-subunit have been isolated from rat brain. The type II form is most predominant in embryonic and neonatal brain, whereas the alternatively spliced form of type II, i.e. type IIA, is most abundant in adult brain (Beckh, Noda, Lübbert & Numa, 1989). The cDNA for the rat brain Na^+ channel β1-subunit has also been cloned (Isom *et al.* 1992). The mRNA encoded by the Na^+ channel type IIA α-subunit, when injected in *Xenopus* oocytes, directs the synthesis of functional Na^+ channels, but with slower inactivation properties. Co-expression of the β1-subunit increases the expression level and accelerates the decay of Na^+ current (Catterall, 1992). Similar results were obtained with the α-subunit of the rat muscle μ1 sodium channel

* To whom correspondence should be addressed.

(Ukomadu & Zhou, 1992). Interestingly, when the rat brain type IIA Na^+ channel α-subunit was expressed in a somatic cell line (Chinese hamster ovary, CHO), the time courses of Na^+ channel relaxation and voltage activation were normal; there is no evidence, however, that these cells express an endogenous $\beta 1$-subunit to form a complex with the transfected α-subunit. Evidently the $\beta 1$-subunits do not have as important a functional impact when the α-subunit is expressed in the genetic background of a mammalian somatic cell line (West, Scheuer, Maechler & Catterall, 1992).

While the *Xenopus* oocyte expression system continues to be used for structure–function studies, the use of mammalian expression systems is being increasingly favoured (Scheuer, Auld, Boyd, Offord, Dunn & Catterall, 1990; Hsu *et al.* 1993). High-level stable expression of rat brain type IIA Na^+ channels in a CHO-K1 cell line has been reported (West *et al.* 1992). But the presence of a low-level endogenous Na^+ current in these cells complicates the quantitative analysis of the current waveform. On the other hand, in CHO cells with a much lower endogenous Na^+ current (Scheuer *et al.* 1990; West *et al.* 1992; Lalik, Krafte, Volberg & Ciccarelli, 1993) relatively high-level expression was only transiently possible using a different expression system (Hsu *et al.* 1993). We have recently reported a high-level stable expression of the rat brain type IIA Na^+ channel α-subunit in CHO cells (Sarkar & Sikdar, 1994). In control electrophysiological studies on untransfected CHO cells we could not observe any detectable levels of endogenous background Na^+ currents. In this paper we describe the analysis of kinetic properties of the same expressed channel according to Hodgkin–Huxley formalism.

METHODS

The rat brain type IIA Na^+ channel α-subunit was expressed in CHO cells. Details of expression for cells stably expressing Na^+ channels, henceforth called CNa18 cells, are described elsewhere (Sarkar & Sikdar, 1994). Patch clamp recordings were done at 15 °C, on CNa18 cells, maintained in Dulbecco's modified Eagle's medium (DMEM)–F12 Ham mixture (Sigma) supplemented with 7% fetal bovine serum (Boehringer Mannheim) in the presence of 300 μg ml^{-1} (active) G418 (an antibiotic; Sigma) in a humidified 5% CO_2 environment, grown to about 60% confluency in 35 mm tissue culture dishes. Temperature was maintained using a TC-202 bipolar temperature controller (Medical Systems Corp., Greenvale, NY, USA). Patch pipettes were pulled from thin-walled omega-dot borosilicate glass capillaries (1·5 mm o.d., Intracel, Royston, Herts, UK). The pipette solution had the following composition (mM): 12 NaCl, 130 CsCl, 5 Hepes, 1 $CaCl_2$ and 10 EGTA (pH 7·4). Choline chloride was used to replace NaCl in the external solution to reduce the amplitudes of the recorded currents and thereby minimize the error due to series resistance. Unless specified otherwise the bath solution contained (mM): 52 NaCl, 85 choline chloride, 5 Hepes, 1 $MgCl_2$, 1·5 $CaCl_2$ and 10 glucose (pH 7·4). Patch pipettes filled with internal solution had resistances of less than 2 MΩ. Whole-cell currents were recorded using a List EPC-7 patch clamp amplifier after capacitance cancellation, about 70% series resistance (R_S) compensation, and filtration at 3 kHz using the built-in circuits of the amplifier. Data were digitized through a CED1401 A/D, D/A converter and stored in a PC-AT 286 computer.

Design and generation of voltage pulses, data acquisition, leak subtraction and preliminary waveform analysis were done using WCP (J. Dempster, University of Strathclyde) as well as WCPA, a version of the same software modified by the authors. The data were sampled at 100 kHz unless specified otherwise. For an optimal signal-to-noise ratio, capacitive and leak currents were subtracted using a modified P/−2 protocol where ten leak records with negative and half-amplitude voltage pulses were used for a set of four test records.

Curve fittings were done on a CDC4360 computer using IMSL subroutine RNLIN with the criterion of 'least squares' for the best fit. Na^+ current relaxation in response to a step depolarization was fitted to Hodgkin–Huxley equations following the method of Keynes & Rojas (1976) and Stühmer *et al.* (1989). In the first step, a point, t_b, in the declining phase of Na^+ current was roughly estimated where the rate of decline of the current was maximum. The process of inactivation was studied by fitting Na^+ current (I_{Na}) beyond t_b with the following equation:

$$I_{Na}(t) = I_1 \exp(-t/\tau_1) + I_2 \exp(-t/\tau_2) + I_3, \quad (1)$$

where τ_1 and τ_2 are time constants of inactivation, I_1 and I_2 are the corresponding amplitudes and I_3 is the steady-state current. Next, the Na^+ current in the initial rising part, i.e. $t < t_b$, was divided by the right-hand side of eqn (1) putting in the values of the parameters, I_1, I_2, I_3, τ_1 and τ_2 obtained from the above fit. Thus we obtain the instantaneous current value, I'_{Na}, defined by the following equation:

$$I'_{Na} = I_{Na}/(I_1 \exp(-t/\tau_1) + I_2 \exp(-t/\tau_2) + I_3). \quad (2)$$

I'_{Na} was then fitted by the following equation:

$$I'_{Na}(t) = \{1 - \exp[-(t - \delta t)/\tau_m]\}^x, \quad (3)$$

keeping instrumental or hyperpolarization-induced delay (δt) and activation time constant (τ_m) as free and x fixed at different integral values, and thereby locating the upper and lower integral limits of the best possible value of x. In the next step, initial values of the fit were adjusted to coincide with the best-fitted parameters corresponding to any one of the two integral limits of x. Then, in addition to the other two parameters, x was set free for best fitting by eqn (3). The mean best-fitted value for x came out, in our case, to be 2. This is further discussed in Results under Activation. In the final step the complete Na^+ current was subjected to a fit by the following form of the Hodgkin–Huxley equation:

$$I_{Na}(t) = I_{ss}\{1 - \exp[-(t - \delta t)/\tau_m]\}^2 \times (a_1 \exp(-t/\tau_1) + a_2 \exp(-t/\tau_2) + a_3), \quad (4)$$

where I_{ss} is the steady-state value of the Na^+ current in the absence of inactivation. The values of the parameters obtained from the fits with eqns (1) and (3) were used as the initial values and it was assumed that the value of the inactivation factor, h, was 1 at the time of onset of the pulse. Parameters determined from this fit were used for further analysis and plotting. Details of other calculations are discussed in the text.

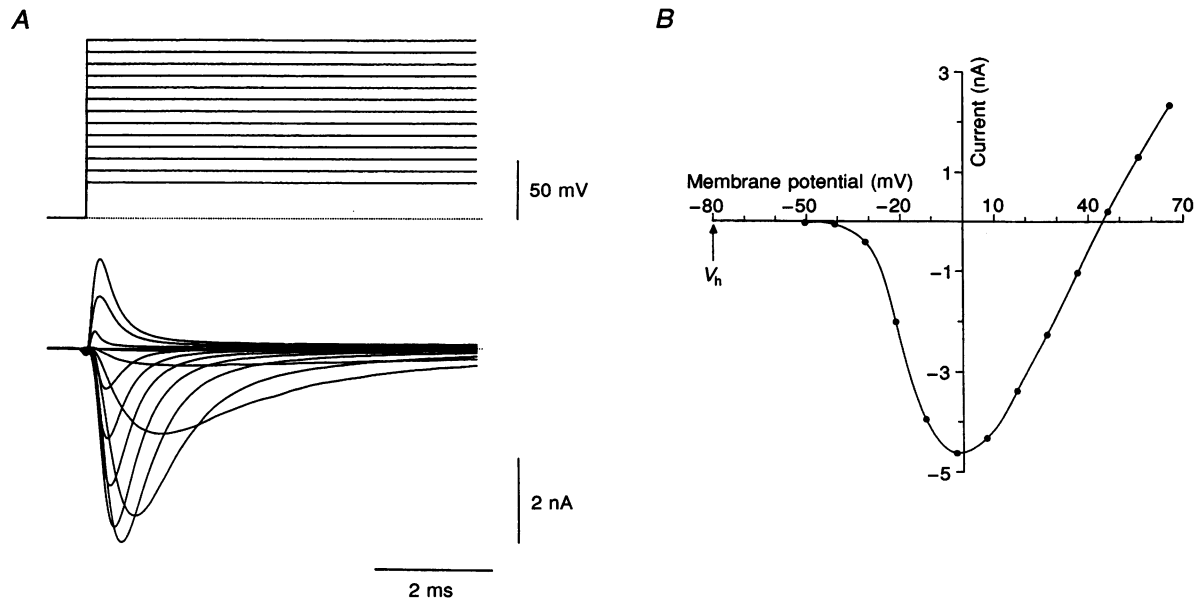

Figure 1. Isolated whole-cell Na^+ current and I_{peak}–V relation

A, voltage (upper) and leak-subtracted current (lower) traces in response to depolarizing pulses. Holding potential (V_h) was −80 mV. The rectangular pulse potential was varied from −50 to +66 mV in 9·7 mV steps. The duration of each pulse was 20 ms. Internal and external Na^+ concentrations were 12 and 85 mM, respectively. *B*, plot of peak Na^+ current *vs.* pulse potential. The current reverses at +45 mV.

RESULTS

Figure 1*A* shows typical traces of Na^+ current, after leak subtraction, in response to depolarizing steps. The current reversed near +45 mV, which is close to the value +48·5 mV, estimated from the Nernst equation. With the composition of the bath and pipette solution given in the previous section, Na^+ current was barely observable at −40 mV. Analysable currents were observed at potentials of −30 mV and above. Figure 1*B* is a plot of peak I_{Na} *versus* membrane potential (V) of the data shown in Fig. 1*A*. The curve is bell shaped with a peak occurring at −5 mV. The CNa18 cells differed widely in the values of the maximum peak current, with a range from 0·5 to 10 nA. However, only currents from cells where the maximum current was less than 8 nA were analysed, so that after compensation the error in the clamping potential due to series resistance was limited to within 3 mV. The current was found to be almost completely blocked by 75 nM TTX.

Inactivation

Development

The time course of the development of inactivation was studied by fitting the declining parts of the Na^+ current

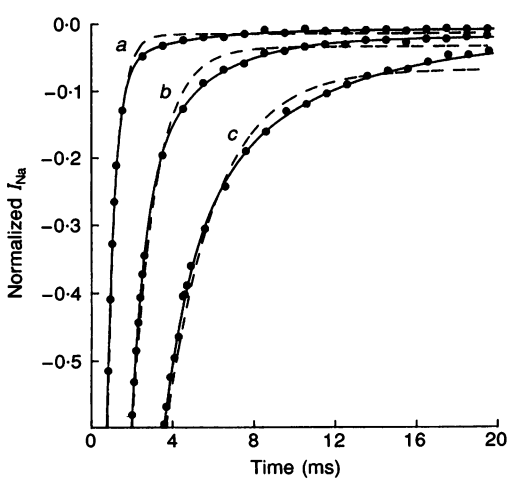

Figure 2. The biphasic nature of Na^+ current inactivation

Declining portions of Na^+ currents (●) elicited at +27 (*a*), −11 (*b*) and −21 mV (*c*) are fitted with single-exponential functions, as in eqn (5) (dashed line) as well as by the sum of two exponentials, given by eqn (1) (continuous line). Each trace was normalized by the maximum value of the Na^+ current in that trace so that they could be plotted on the same scale. Although the experimental data were collected and analysed at regular intervals of 10 μs, for clarity of presentation only one out of 10–20 points in the initial region and one out of 100 points in the latter part, are presented in the plot. The inactivation is better described by the sum of two exponentials.

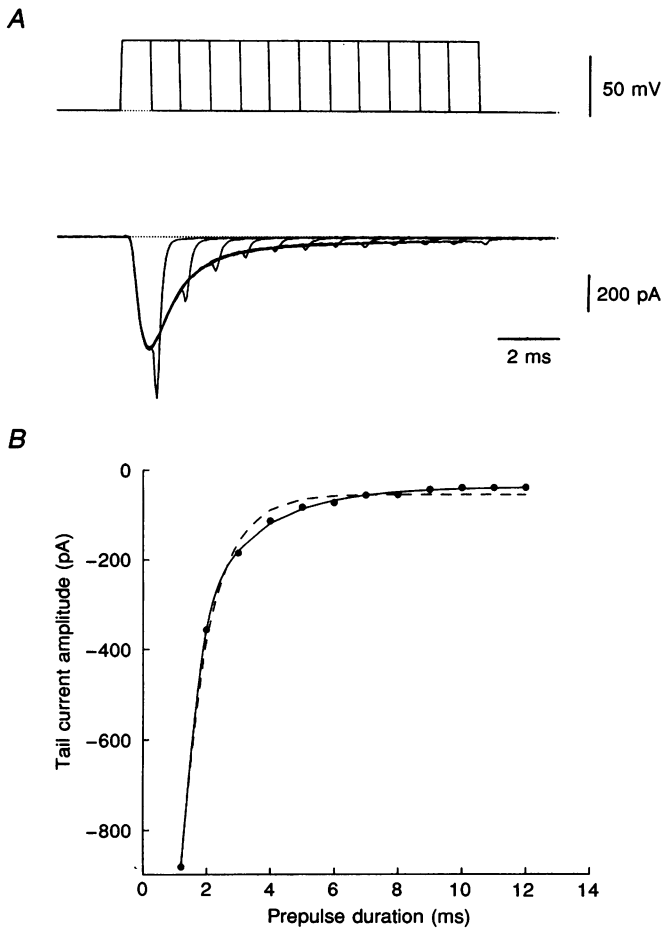

Figure 3. The time course of the development of inactivation

Inactivation was studied from the gradual reduction of the peak of the tail current in response to a voltage protocol shown in the upper trace of *A*. Holding potential was −80 mV. A series of rectangular pulses to 0 mV was applied with increasing duration, starting from 1 ms and with a step of 1 ms. The leak-subtracted current response is shown in the lower trace. *B*, the peak of the tail current (●) is plotted against the duration of the voltage pulse. The dashed curve shows the fit with a single exponential (eqn (5) in text), while the continuous curve shows the fit with the sum of two exponentials (eqn (1) in text).

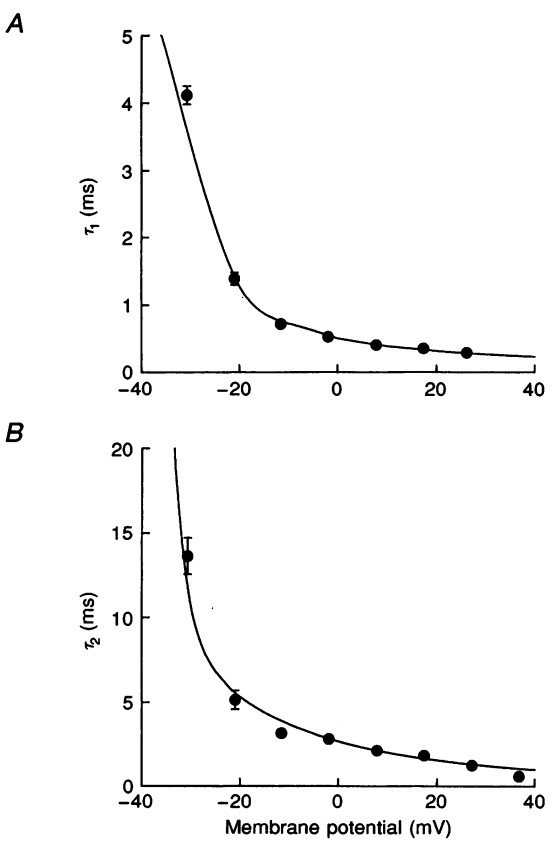

Figure 4. Plot of inactivation time constants against membrane potential

The smaller (τ_1) and larger (τ_2) time constants of inactivation are plotted in *A* and *B*, respectively. Each point represents the mean of 12 independent experiments. Error bars (± S.E.M.) are shown where larger than the symbol. The continuous lines are drawn using eqns (12) and (13) in the text.

traces, elicited in response to 20 ms depolarizing pulses to different potentials as shown in Fig. 1*A*, with exponential functions. The Hodgkin–Huxley model predicts that the decay of the current would be monoexponential, i.e. of the form:

$$I_{Na}(t) = I_1 \exp(-t/\tau_h) + I_0, \quad (5)$$

where I_1 is the current amplitude and I_0 is the steady-state current. However, our data, in the range of −30 to 40 mV, were not well fitted by eqn (5) even after allowing a very high steady-state value. This is illustrated in Fig. 2 for three different depolarization potentials. The deviation from monoexponentiality, however small, was consistent at all potentials and was found in at least fifty cells so far observed. The data were fitted much better with the sum of two exponentials of the form given by eqn (1). We have performed a statistical test on these fits as suggested by Horn (1987). We found that with the monoexponential model as null and the biexponential model as the alternative hypothesis the P value turns out to be very small and the alternative model is acceptable, even at a 0·0001 level of significance. On the other hand, when the same data were fitted by a sum of three exponentials, taking the two-exponential model as the null hypothesis and the three-exponential model as the alternative, the improvement in the fit was very low even when the level of significance was set to 0·1. Therefore, a two-exponential fit for the inactivation process was statistically acceptable. The deviation from monoexponentiality was not an artifact due to uncompensated access resistance for the following reasons. (1) The existence of the second component was not influenced by the degree of R_S compensation. The amplitude of this component was the same whether the series resistance was uncompensated or properly compensated. (2) CNa18 cells differed widely in the magnitude of the Na^+ current. However, the relative amplitudes of the exponential components and the time constants of inactivation did not depend on this magnitude. (3) The relative amplitudes of the exponentials and the time constants were insensitive to variation in the concentration of Na^+ in the external or internal solution. However, the fast component of inactivation was found to dominate the process of inactivation. The relative amplitude, a_1, of the fast component increased with the pulse potential, varying from 0·67 to 0·97 in the potential range of −30 to +40 mV.

The time course of the development of inactivation was also studied from the reduction in tail current amplitude on increasing the duration of the pulse as described in the legend of Fig. 3. The plot of the peak tail current against the duration of the prepulse was also better fitted by eqn (1) than eqn (5), supporting a two-exponential inactivation process. Figure 4 shows the variation of these two time constants determined from the fit of the declining phase of the Na^+ current against potential. The magnitude and the potential dependence of the fast component matched well with the usual fast inactivation of the Na^+ current reported earlier (Hodgkin & Huxley, 1952; Bezanilla & Armstrong,

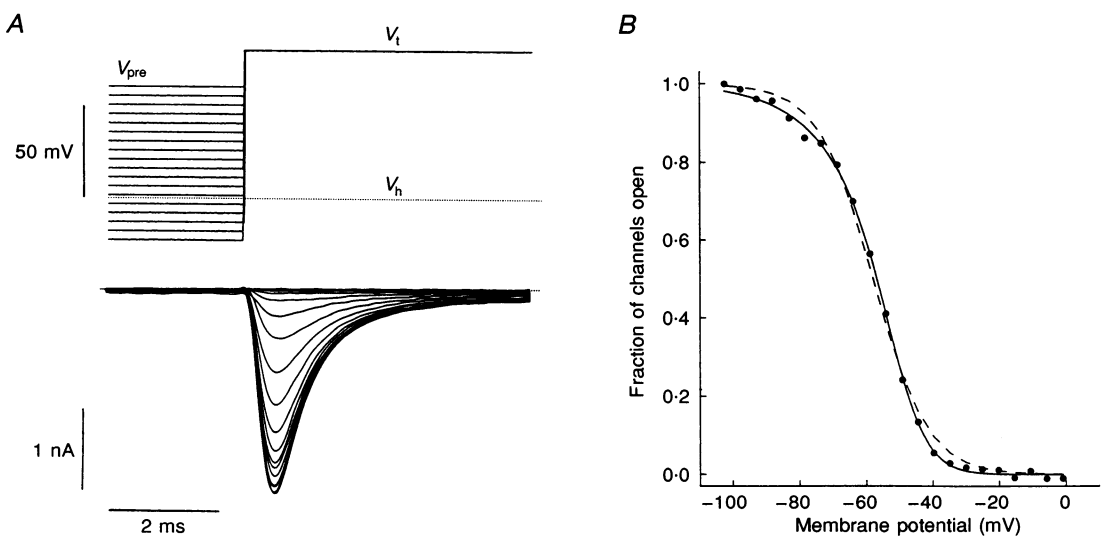

Figure 5. Steady-state inactivation

The upper set of traces in *A* shows the voltage protocol used to study the steady-state probability of inactivation. A prepulse to V_{pre} of duration 500 ms was applied, immediately followed by a test pulse to V_t (0 mV, 20 ms). V_{pre} was varied from −102 to −1 mV in 4·8 mV steps. The lower set of traces are the leak-subtracted currents. For clarity, voltage and current traces up to V_{pre} of −20 mV are shown. Peak currents at test pulses were normalized by their maximum value, observed when the prepulse was at −102 mV, and plotted against prepulse potential in *B*. The dashed curve shows the best fit with eqn (6) in the text, while the continuous curve is the best fit with eqn (7). The best fitted values of V_1, V_2, k_1 and k_2 are −50·04, −52·184, 13·18 and 4·74 mV, respectively.

1977; Aldrich, Corey & Stevens, 1983; Scheuer *et al.* 1990). However, this component was not as fast and as steeply voltage dependent as observed by Belluzzi & Sacchi (1991) or Howe & Ritchie (1992) for the rat sympathetic neuron and rabbit Schwann cells, respectively, and as calculated from the Armstrong & Gilly (1979) model of Na^+ channels by Keynes (1991). On the other hand, the slow component of inactivation is different from the so-called *slow* inactivation, in which the time constant is reported to be in the order of seconds (Adelman & Palti, 1969; Chandler & Meves, 1970; Belluzzi & Sacchi, 1991; Starkus, Rayner, Fleig & Ruben, 1993).

Steady state

The steady-state probability of inactivation was investigated using a protocol described in the upper trace of Fig. 5*A*. The peak current in each test pulse is proportional to h_∞, the fraction of channels remaining uninactivated at the end of the prepulse. Figure 5*B* is the plot of h_∞ against membrane potential. If one assumes that the process of inactivation involves only two states, variation of the steady-state probability with potential should follow a Boltzmann distribution given by:

$$h_\infty = 1/\{1 + \exp[(V - V_0)/k]\}, \quad (6)$$

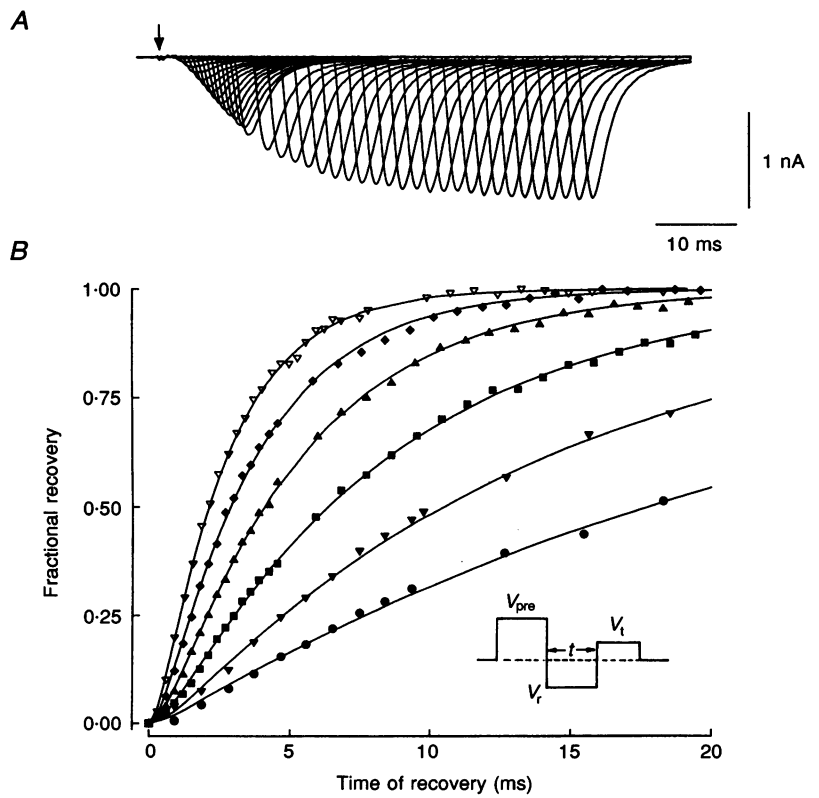

Figure 6. Recovery from inactivation

The time course of recovery of the channels from inactivation was studied using a voltage protocol described schematically in the inset of *B*. Channels were completely inactivated by a 50 ms depolarizing pulse, V_{pre}, to +30 mV and then held at a level V_r for different durations followed by a step to the level V_t (−10 mV, 10 ms). Recovery was studied at V_r ranging from −70 to −120 mV. *A* illustrates a series of current traces when V_r was at −80 mV. The arrow shows the point at which the potential was switched to V_r from V_{pre}. The peak current at the test potential increased with the time of recovery, i.e. as the duration of V_r increased, finally attaining a steady-state value. Peak currents at a constant V_r but of different durations were measured, normalized by the steady-state value, and plotted against the time of recovery in *B*. Different symbols represent observations at different V_r (●, −70 mV; ▼, −80 mV; ■, −90 mV; ▲, −100 mV; ◆, −110 mV; ▽, −120 mV). The time of recovery was varied from 0·94 to 9·4 ms by 0·94 ms steps and then up to 106 ms by 3 ms steps when V_r was −70 or −80 mV. At more hyperpolarized recovery potentials the first few milliseconds of data were collected using a step of 0·3 ms and later the step was increased to 0·88 ms. Data were sampled at 60 μs intervals for this experiment. The continuous lines were fitted using eqn (8). Values of the recovery time constants from the above fit were as follows. τ_1: 0·527, 0·699, 0·636, 0·619, 0·479 and 0·388 ms at V_r of −70, −80, −90, −100, −110 and −120 mV, respectively. τ_2 at the same potentials: 24·879, 14·099, 8·258, 4·961, 3·444 and 2·469 ms, respectively.

where V is the prepulse potential, V_0 is the membrane potential at half-maximal inactivation and k is the slope factor. The dashed curve shows the best fit with eqn (6). Evidently the fit is not satisfactory. If, on the other hand, one assumes that the inactivation gate has three distinct states, the Boltzmann distribution is given by the form:

$$h_\infty = 1/\{1 + \exp[(V - V_1)/k_1] + \exp[(V - V_2)/k_2]\}, \quad (7)$$

where V_1 and V_2 are the membrane potentials at half-maximal inactivation. The continuous curve is the best fit with eqn (7). This result further supports the existence of a three-state inactivation process.

Recovery from inactivation

The time course of recovery of the channels from inactivation was studied as described in the legend to Fig. 6. The normalized peak current in the test pulse, $F(t)$, represents the fraction of channels recovered from inactivation relative to its steady-state value. At all values of V_R, a delay before the onset of recovery was observed which clearly indicates that the process of recovery is not given by a single exponential. Therefore, a double-exponential form was tried. The most general form of the double exponential is given by eqn (1) after imposing the following constraints: (1) the fraction of open channels, $F(t)$, is zero at the recovery time, $t = 0$; (2) the steady-state value of $F(t)$ is 1, which, follows from the definition; and (3) the slope of the $F(t)$ curve is zero at $t = 0$ (i.e. there is a delay in the onset of recovery). The same equation takes the form:

$$F(t) = 1 + \frac{\tau_1}{(\tau_2 - \tau_1)} \exp(-t/\tau_1) - \frac{\tau_2}{(\tau_2 - \tau_1)} \exp(-t/\tau_2). \quad (8)$$

The continuous line was fitted using eqn (8). The fits were quite satisfactory. The presence of the fast component was responsible for the delay, i.e. its amplitude was positive while the slower component dominated the process. Both time constants of recovery were found to decrease with potential, unlike the formation of a plateau that was calculated from the model of Armstrong & Gilly (1979) by Keynes (1991).

Potential dependence of single-channel current

The dependence of single Na^+ channel current (i) on membrane potential was investigated through the instantaneous current–voltage relationship as shown in Fig. 7. The dashed line is the best-fitted linear ohmic relation whereas the continuous line represents a fit with the constant-field equation:

$$i(V) = P_{Na} \frac{F^2 V}{RT} [Na^+]_o \frac{\exp[F(V - V_{Na})/RT] - 1}{\exp(FV/RT) - 1}, \quad (9)$$

where F is the Faraday constant, R is the gas constant, T is the absolute temperature and $[Na^+]_o$ is the external concentration of Na^+. V_{Na} is the Nernst equilibrium potential for sodium. Na^+ permeability, P_{Na}, was the only free parameter of the fit. For the data shown in Fig. 7, the best fitted value of P_{Na} was determined to be $2{\cdot}83 \times 10^{-10}$ cm^3 s^{-1}. For further analysis, the potential dependence of the single-channel current was assumed to follow eqn (9).

Activation

Time dependence

The numerical method to investigate the activation dynamics is discussed in Methods. The transformed current I'_{Na} was fitted by eqn (3). The fitted value of δt did not show any correlation with the pulse potential. Its value was limited to within a few tens of microseconds and increased rather weakly with the peak value of I_{Na}. The value of δt was strongly dependent on the degree of R_S compensation, increasing up to 850 μs in uncompensated conditions. The effect of hyperpolarization on the Na^+ current relaxation was studied by varying the holding potential from −60 to −120 mV. We did not find any systematic effect of holding

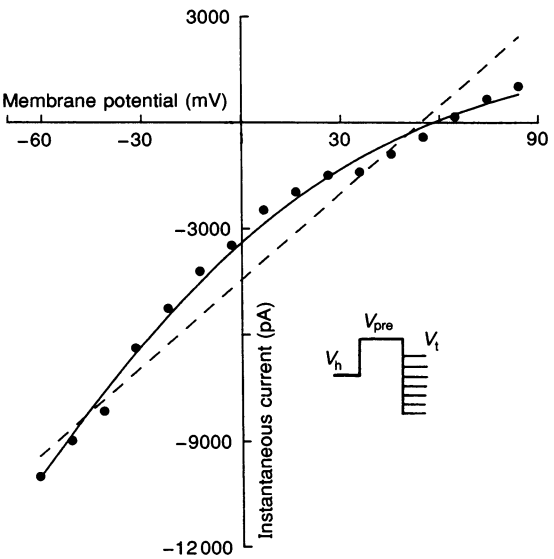

Figure 7. Instantaneous current–voltage relationship
The inset shows the voltage protocol. A 1 ms prepulse to 0 mV was applied prior to a test pulse of 10 ms to values of V_t ranging from −61 to +84 mV with 9·7 mV steps. After leak subtraction, the current at the test pulse was extrapolated back to the time of onset of V_t. The extrapolated current is plotted against V_t in the figure (●). The dashed line is the best fitted straight line whereas the continuous line represents the fit with the constant-field equation (eqn (9)). Internal and external Na^+ concentrations were 11 and 127 mM, respectively. It may be noted that the reversal potential of the current was higher in this experiment compared with that observed in Fig. 1, which actually demonstrates that the current is sensitive to the external Na^+ concentration.

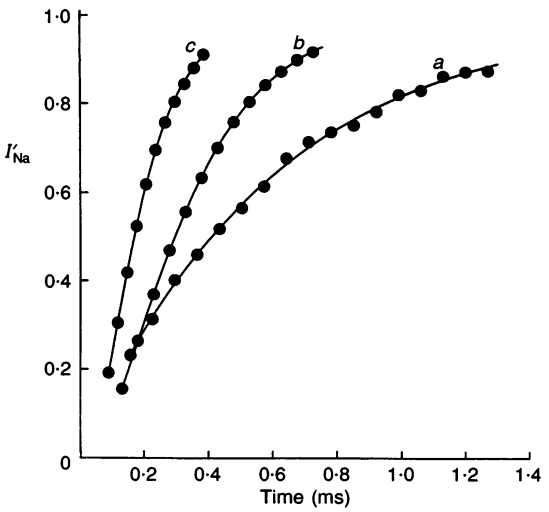

Figure 8. Activation of Na^+ current

Normalized I'_{Na} and its fit with eqn (3) are plotted against time for different pulse potentials: −31 (*a*), −2 (*b*) and +37 mV (*c*). The best fitted values of the power x are 0·97, 2·05 and 2·66, respectively (see text for details). The number of experimental points shown on the plot was adjusted to maintain a uniform density.

potential on the time course of Na^+ current, although the amplitude increased with hyperpolarizations with a minor (less than 3 μs per 10 mV depolarization) and/or non-monotonic variation in the delay factor, δt. Thus we can interpret this delay as coming from the instrumental source and not from the same source as reported by Keynes & Rojas (1976).

The best-fitted value of x in eqn (3) was not unique and rather dependent on the membrane potential. An improper R_S compensation may affect the activation kinetics. However, the results of activation kinetics were independent of the magnitude of the Na^+ current. Table 1 gives the values of x at different membrane potentials for twelve different cells and the maximum Na^+ current observed with these cells. A tenfold variation in the maximum Na^+ current observed did not show any correlation with the estimated value of x. Moreover, $I_{peak}-V$ plots (similar to Fig. 1*B*) for these twelve cells were superimposable after scaling. The values of τ_m determined for these cells did not show any dependence on the magnitude of the Na^+ current. Therefore, the results are unlikely to be influenced much by the R_S compensation error. Figure 8 shows the fits of I'_{Na} with eqn (3) at three different potentials. The nearest integer to the mean of x taken over all the potentials was 2. The dynamics of the channel could thus be approximated by m^2 in the Hodgkin–Huxley formalism. For further analysis, whole Na^+ current traces were fitted with eqn (4) with the value of x fixed at 2. Figure 9 shows three such fits. The values of τ_m obtained from the latter fits are plotted against potential in Fig. 10*A*. As observed by others (Hodgkin & Huxley, 1952; Belluzzi & Sacchi, 1991), τ_m was found to be a decreasing function of the depolarization potential within the range of observation.

Steady-state activation

The steady-state permeabilities, P_{Na}, were estimated from I_{ss} (eqn (4)), the steady-state value of the Na^+ current in the absence of inactivation, and corrected for instrumental delay at each potential and normalized by its maximum value. Normalized permeabilities were the measure of p_∞,

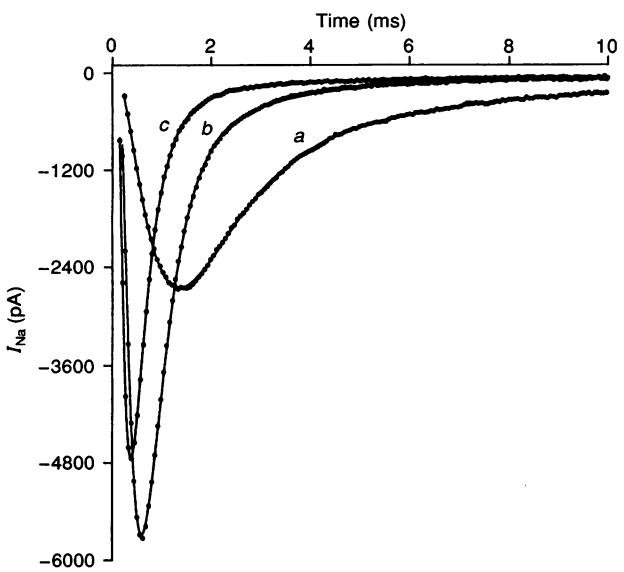

Figure 9. Fit of Na^+ current trace with Hodgkin–Huxley model

I_{Na} fitted with eqn (4) (at potentials of −21 (*a*), −2 (*b*) and +18 mV (*c*)), the modified Hodgkin–Huxley equation. One out of six experimental points (●) are shown on the plot. The continuous line shows the fit.

Table 1. The best value of the power x, from fits with eqn (3)

Cell	$I_{Na,max}$ (pA)	x at different membrane potentials							
		−31 mV	−21 mV	−11 mV	−2 mV	8 mV	18 mV	27 mV	37 mV
1	754	0·86	1·90	2·70	2·60	2·32	2·10	2·60	1·85
2	1084	0·97	2·60	1·50	2·07	2·40	2·53	2·60	1·98
3	1086	1·30	1·44	2·83	2·50	2·65	2·63	1·90	2·12
4	1133	0·81	1·40	1·70	2·70	2·08	2·41	1·59	2·24
5	1191	1·20	1·22	2·10	2·63	2·15	1·78	2·41	1·20
6	1218	1·33	1·46	2·07	2·31	2·34	2·53	2·82	2·20
7	1646	0·92	1·74	2·20	2·31	2·30	1·65	3·00	3·40
8	2192	0·89	1·45	2·28	2·63	2·80	2·70	2·50	2·80
9	2402	0·60	1·84	2·15	2·36	2·38	2·67	3·50	2·20
10	4626	1·29	1·79	1·96	2·34	2·38	2·59	1·74	1·78
11	5728	0·87	1·72	1·86	2·02	2·46	2·34	2·63	2·61
12	7358	0·86	1·83	3·00	2·40	1·89	1·44	1·62	1·80
Mean		0·99	1·69	2·19	2·41	2·34	2·28	2·41	2·18
S.E.M.		0·01	0·11	0·13	0·06	0·07	0·13	0·17	0·16

$I_{Na,max}$, maximum Na^+ current in the cell.

the steady-state open probability, and were plotted against potential in Fig. 11, to yield the activation curve. The sigmoidal curve was fitted with the Boltzmann equation:

$$P_{Na}/P_{Na,max} = 1/\{1 + \exp[(V - V_{½})/k]\}, \quad (10)$$

where V is the membrane potential and $V_{½}$ is the membrane potential at half-maximal activation. The value of the gating charge from this fit was estimated to be $3{\cdot}227e$. The inset to Fig. 11 shows the activation plot in a logarithmic scale for the same data. The gating charge estimated from the limiting slope was $4{\cdot}7e$. Considering the deviation of data points from the fitted line at higher potentials, fits by either the sum of two Boltzmann distributions or a Boltzmann distribution similar to eqn (7) were tried. However, improvements of the fits over the single Boltzmann distribution were not statistically acceptable at a 0·01 level of significance. Further, there was no improvement in the kinetic description assuming a multiexponential form of the variable m or the sum of two m variables.

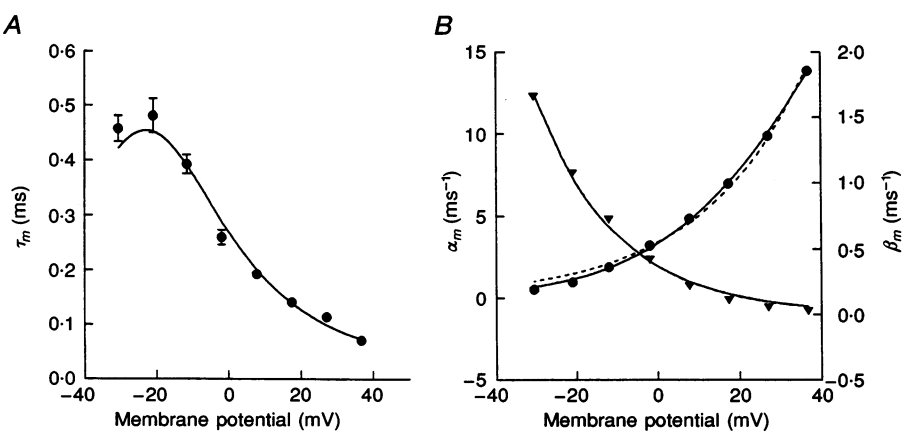

Figure 10. Plots of τ_m and the activation rate constants, α_m and β_m, *versus* membrane potential

A, plot of τ_m against membrane potential. Each point is a mean of 12 independent experiments with error bars (± S.E.M.) shown. The continuous curve was drawn using the equation $\tau_m = 1/(\alpha_m + \beta_m)$, where the voltage dependences of α_m and β_m are given by eqns (16) and (17). *B*, plot of α_m (●) and β_m (▼) against potential. Dashed curves represent fits with eqn (16). The continuous curves, on the other hand, represent fits with the form given in eqn (17). In the case of α_m the fit was much better with the second form, whereas for β_m the fits are indistinguishable. With the first form the values of the fits are α^0_m, 3·384 ms^{-1} and β^0_m, 0·371 ms^{-1}; the values of z are 0·959 and 1·224, respectively. The values of the constants A, B and C for the α_m fit are 22·763 ms^{-1}, −13·67 mV and 0·628 mV respectively.

DISCUSSION

Rat brain type IIA Na^+ channel α-subunits, stably expressed in CHO cells, yielded a TTX-sensitive transient Na^+ current with a typically bell-shaped I_{peak} *vs.* V plot (Fig. 1). The peak of this plot was around −5 mV. Earlier reports of this value for the same cDNA expressed in CHO-K1 cells was −10 to −20 mV (West *et al.* 1992). As the cDNA was isolated from total rat brain we cannot identify a native neuronal environment of the original and intact channel. However, we can compare it with the results from the cultured rat hippocampal neuron (Staffan & Århem, 1992) where the peak of the $I_{peak}-V$ curve has been reported to occur at −10 mV.

In comparison with the classical Hodgkin–Huxley model, the first difference in the kinetics of Na^+ channels of CNa18 cells concerns inactivation. The time courses of both the formation of, and recovery from, inactivation were given by the sum of two exponentials rather than a single exponential. The steady-state inactivation was also much better fitted by eqn (7), a Boltzmann distribution assuming three states between the non-inactivated and the inactivated state. The fast inactivation was quite comparable to that of the other systems including RIIA α-subunit expressed in CHO (Hsu *et al.* 1993). τ_2 of inactivation, in our case, is only four to five times larger than τ_1. Therefore it can be termed *intermediate* inactivation, or inactivation of group B as classified by Howe & Ritchie (1992). Intermediate inactivation has been observed in other biological systems (Chiu, 1977; Ochs, Bromm & Schwartz, 1981; Neumcke & Stämpfli, 1982; Howe & Ritchie, 1992; Hebert, Monette, Dunn & Drapeau, 1994). It is interesting to note that the α-subunit of μ1 Na^+ channels expressed in HEK 293 cells also shows similar *intermediate* inactivation (Ukomadu & Zhou, 1992). Contrary to our results, however, for quite a similar preparation, Hsu *et al.* (1993) did not find this intermediate component of inactivation and West *et al.* (1992) found the steady-state inactivation to be well fitted by eqn (6). On the other hand, with a mutant variant of the type IIA clone (VA200), expressed in *Xenopus* oocytes, a fast and an *intermediate* component of inactivation similar to our results have been reported (Krafte, Goldin, Auld, Dunn, Davidson & Lester, 1990). These discrepancies may be attributed to the different expression techniques used. While Hsu *et al.* (1993) used the vaccinia virus expression system, West *et al.* (1992) used CHO-K1 cells and a vector with a metallothionein promoter. The observation of fast and intermediate time constants could also be attributed to partial dephosphorylation of the channel proteins as there was no control on phosphorylation under our experimental conditions. Recent studies on the same channel protein have suggested the role of phosphorylation in stabilizing distinct gating modes of Na^+ channels (Numann, Catterall & Scheuer, 1991; Fleig, Ruben & Rayner, 1994). Hebert *et al.* (1994) have recently proposed that the inactivation components originate from two separate gating modes of Na^+ channels and switching between the fast and a slower

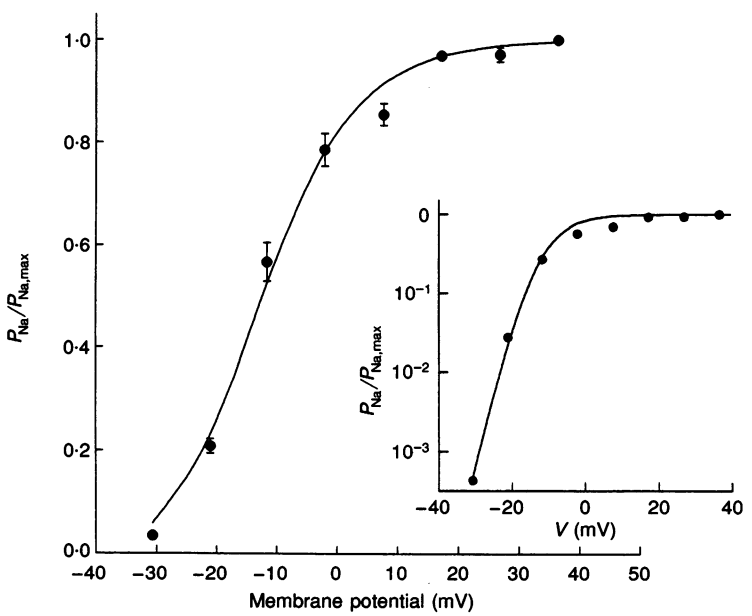

Figure 11. $P_{Na}/P_{Na,max}$ plotted against potential

Each point is the mean of 12 independent experiments with error bars (± S.E.M.) shown. The continuous line is the fit with Boltzmann eqn (10). Values of $V_{½}$ and k are −11·94 and −7·7 mV, respectively. Inset shows the plot of $P_{Na}/P_{Na,max}$, on a log scale, *vs.* potential. The limiting logarithmic slope is 5·3 mV per e-fold change, owing to a gating charge of 4·67e.

mode depends on the expression level. A higher level of expression selects for the fast mode. However, our data fail to support this idea as the level of expression in CNa18 cells did not have any effect on the relative amplitude of the exponentials in the inactivation.

A three-state scheme for inactivation

The Hodgkin–Huxley model for the Na^+ channel assumes a two-state process for inactivation that is not supported by our experimental results. It needs a three-state scheme to explain the results with a minimal modification of the Hodgkin–Huxley model. Ochs *et al.* (1981) suggested a way to discriminate between different alternative three-state models. Four linear three-state schemes can be considered:

$$O \rightleftharpoons I_1 \rightleftharpoons I_2, \qquad \text{Scheme 1}$$

$$O_1 \rightleftharpoons O_2 \rightleftharpoons I, \qquad \text{Scheme 2}$$

$$O_1 \rightleftharpoons I \rightleftharpoons O_2, \qquad \text{Scheme 3}$$

$$I_1 \rightleftharpoons O \rightleftharpoons I_2. \qquad \text{Scheme 4}$$

In these schemes O denotes the non-inactivated state and I denotes the inactivated state. The time constants and relative amplitudes of exponentials in both the formation and recovery kinetics may be calculated from each of these schemes. Assuming the rate constants to be either monotonically increasing or decreasing with potential, as dictated from the scheme, one can calculate the asymptotic behaviour of the model parameters under conditions of extreme depolarization and hyperpolarization. From these calculations, schemes 2 and 3 may be eliminated because both of them predict that the fast exponential is the dominating component in the recovery process in strongly hyperpolarized conditions whereas we observed the reverse to be true. According to scheme 4 the amplitude of the fast component in the recovery process is negative, while from experiments it appears to be positive. In other words, scheme 4 cannot account for the delay in the recovery. On the other hand, asymptotic behaviour of scheme 1 conforms to the experimental observations. A similar scheme was proposed by Chiu (1977) for frog neuronal Na^+ channels. Recently, a synthetic peptide containing the Ile–Phe–Met sequence was found to simulate inactivation in non-inactivating Na^+ channels by causing a frequency-dependent open channel block (Eaholtz, Scheuer & Catterall, 1994), supporting the hypothesis that the sequence IFM serves as the inactivation particle of the Na^+ channel. However, the above results also suggest that, besides the block by the inactivation particle, there is one more step in the process of inactivation that is responsible for the reduction of tail current in the normal inactivating Na^+ channel. Two sequential states of inactivation as shown in scheme 1 may, therefore, be considered.

Determination of the rate constants corresponding to scheme 1

Four rate constants are associated with scheme 1 in the following way:

$$O \underset{a_{10}}{\overset{a_{01}}{\rightleftharpoons}} I_1 \underset{a_{21}}{\overset{a_{12}}{\rightleftharpoons}} I_2 \qquad \text{Scheme 1}$$

The time constants τ_1 and τ_2 , $h(\infty)$ (the steady-state value of $h(t)$) and a_1 (the amplitude of the fast component) can be expressed in terms of these four rate constants using a Q-matrix formalism (Colquhoun & Hawkes, 1977). The rate constants were thus solved using the experimental values of τ_1, τ_2, $h(\infty)$ and a_1 at each potential. It was found that the potential dependence of the rate constants was much better described by equations such as:

$$a_{ij} = A_{ij} \frac{B_{ij} - V}{1 - \exp\left(-(B_{ij} - V)/C_{ij}\right)}, \qquad (11)$$

than by single exponential functions. Values of $(A–C)_{ij}$ thus obtained are: A_{01}, $-0{\cdot}06188\ ms^{-1}$; B_{01}, $-31{\cdot}34$ mV; C_{01}, $-2{\cdot}067$ mV; A_{10}, $0{\cdot}00114\ ms^{-1}$; B_{10}, $17{\cdot}38$ mV; C_{10}, $0{\cdot}35311$ mV; A_{12}, $-0{\cdot}02924\ ms^{-1}$; B_{12}, $13{\cdot}07$ mV; C_{12}, $-18{\cdot}681$ mV; A_{21}, $0{\cdot}00020\ ms^{-1}$; B_{21}, $-4{\cdot}7479$ mV; C_{21}, $3{\cdot}8608$ mV. These values were used to draw the continuous lines in Fig. 4 using the equations:

$$\tau_1(V) = 2/[\xi_1 + \sqrt{(\xi_1^2 - 4\xi_2)}] \qquad (12)$$

and

$$\tau_2(V) = 2/[\xi_1 + \sqrt{(\xi_1^2 - 4\xi_2)}], \qquad (13)$$

where

$$\xi_1 = a_{01} + a_{10} + a_{12} + a_{21} \qquad (14)$$

and

$$\xi_2 = a_{10}a_{21} + a_{01}a_{21} + a_{10}a_{12}. \qquad (15)$$

(ξ_1^2 is the square of ξ_1.) For the axonal Na^+ channel of the frog *Rana pipiens*, Chiu (1977) found the rate constants to be fitted satisfactorily by the single exponential function. On the other hand, for the axonal Na^+ channel of *Rana esculenta*, the form given in eqn (11) was found to be appropriate (Ochs *et al.* 1981). It is also relevant to note that the Hodgkin–Huxley descriptions of α_m, α_n and β_h are equivalent to eqn (11) (Hodgkin & Huxley, 1952). Patlak (1991) also finds that a strict monoexponential nature of the rate constant is not feasible.

Instantaneous current and activation

From the instantaneous current–voltage relationship, Hodgkin & Huxley (1952) observed that, for the squid giant axon Na^+ channel, the single-channel current can be written as $\gamma(V - V_{Na})$, V_{Na} being the Nernst potential.

Later studies, using more sensitive measurements employing the same technique on a similar preparation failed to confirm this ohmic nature (Keynes & Rojas, 1976). Evidence favouring the constant-field model for the single-channel current is prevalent (Vandenberg & Bezanilla, 1991; Staffan & Århem, 1992). The results of our present study show that the channel is not ohmic and the instantaneous I–V can be described by the constant-field model as in eqn (9).

Analysis of activation kinetics showed that the time course was described by the Hodgkin–Huxley equation of the form given by eqns (3) and (4). The power factor x was not unique but its mean value varied from 1 to 2·4 (see Table 1) with potentials in the range −30 to +40. Similar results are reported for other preparations (Neumcke & Stämpfli, 1982). As the mean value of x is 2, the dynamics can be approximated by m^2 instead of the classical m^3 term in the Hodgkin–Huxley model. A similar observation has been made in many other systems (Dodge & Frankenhaeuser, 1959; Frankenhaeuser, 1960; Brussard, Lodder, Maat, Devlinger & Kits, 1991) including the cultured rat hippocampal neuron (Staffan & Århem, 1992).

Our estimate of the gating charge from the logarithmic plot of activation is ~4·7e. Earlier reports of this value from linear activation plots was 3·93e (West *et al.* 1992) for similar preparations. The original estimate by Hodgkin & Huxley (1952) was 6e. Later, values of ~4e were reported (Keynes & Rojas, 1976; Ruben, Starkus & Rayner, 1990). Our value seems to be somewhat higher. Theoretically, the slope of the logarithmic plot of the activation curve should be equal to the gating charge at extreme negative potentials. Non-availability of data points at potentials below −30 mV, where Na^+ currents could not be elicited, might have affected the extrapolation. Figure 10B shows the plot of the activation rate constants α_m and β_m calculated from m_∞ and τ_m. The dashed curves represent fits with equations of the form:

$$s_m = s_m^0 \exp(zFV/RT), \quad (16)$$

where s stands for α or β and s_m^0 is the value of s_m at $V = 0$. The continuous curves, on the other hand, represent fits of the form:

$$s_m = A(B - V)/\{1 - \exp[-(B - V)/C]\}. \quad (17)$$

In the case of α_m, the fit is much better with the second form, whereas for β_m the fits are indistinguishable. With eqn (16), the values of the fits are $\alpha_m^0 = 3{\cdot}384$ ms^{-1} and $\beta_m^0 = 0{\cdot}371$ ms^{-1} and the values of z are 0·959 and −1·224. These values were used to estimate the effective charge transfer, z_s, and the asymmetry factor, d, of the energy barrier of the transition; the values were: z_s, 2·18 and d, 0·44. Patlak (1991) proposed these values as 2·45 and 0·6. The values of A, B and C for α_m are −0·63 ms^{-1}, 22·76 mV and −13·76 mV, respectively. Hodgkin & Huxley (1952) also described α_m by eqn (17) and the values of the parameters, in their case, were −0·1 ms^{-1}, −35 mV and −10 mV.

In conclusion, the α-subunit of the rat brain type IIA Na^+ channel stably expressed in CHO cells gives rise to a Na^+ channel which functions kinetically, to a large extent, like a native myelinated neuronal Na^+ channel. The function of β-subunits in modulating the properties of the Na^+ channel have yet to be investigated.

Adelman, W. J. & Palti, Y. (1969). The effects of external potassium and long duration voltage conditioning on the amplitude of sodium currents in the giant axon of the squid, *Loligo peali*. *Journal of General Physiology* **54**, 589–606.

Aldrich, R. W., Corey, D. P. & Stevens, C. F. (1983). A reinterpretation of mammalian sodium channel gating based on single channel recording. *Nature* **306**, 436–441.

Armstrong, C. M. & Gilly, W. F. (1979). Fast and slow steps in the activation of sodium channels. *Journal of General Physiology* **74**, 691–711.

Beckh, S., Noda, M., Lübbert, H. & Numa, S. (1989). Differential regulation of three sodium channel messenger RNAs in the rat central nervous system during development. *EMBO Journal* **8**, 3611–3616.

Belluzzi, O. & Sacchi, O. (1991). A five-conductance model of the action potential in the rat sympathetic neurone. *Progress in Biophysics and Molecular Biology* **55**, 1–30.

Bezanilla, F. & Armstrong, C. M. (1977). Inactivation of the sodium channel. I. Sodium current experiments. *Journal of General Physiology* **70**, 549–566.

Brussard, A. B., Lodder, J. G., Maat, A. T., Devlinger, T. A. & Kits, K. S. (1991). Inhibitory modulation by FMRFamide of the voltage gated sodium current in identified neurons in *Lymnaea stagnalis*. *Journal of Physiology* **441**, 385–404.

Catterall, W. A. (1992). Cellular and molecular biology of voltage gated sodium channels. *Physiological Reviews* **72**, S15–48.

Chandler, W. K. & Meves, H. (1970). Slow changes in membrane permeability and long lasting action potentials in axons perfused with fluoride solutions. *Journal of Physiology* **211**, 707–728.

Chiu, S. Y. (1977). Inactivation of sodium channels: second order kinetics in myelinated nerve. *Journal of Physiology* **273**, 573–596.

Colquhoun, D. & Hawkes, A. G. (1977). Relaxation and fluctuations of membrane currents that flow through drug-operated channels. *Proceedings of the Royal Society* B **199**, 231–262.

Dodge, F. A. & Frankenhaeuser, B. (1959). Sodium currents in myelinated nerve fibre of *Xenopus laevis* investigated by the voltage clamp technique. *Journal of Physiology* **148**, 188–200.

Eaholtz, G., Scheuer, T. & Catterall, W. A. (1994). Restoration of inactivation and block of open sodium channels by an inactivation gate peptide. *Neuron* **12**, 1041–1048.

Fleig, A., Ruben, P. C. & Rayner, M. D. (1994). Kinetic mode switch of rat brain IIA sodium channels in *Xenopus* oocytes excised macropatches. *Pflügers Archiv* **427**, 399–405.

Frankenhaeuser, B. (1960). Quantitative description of sodium currents in myelinated nerve fibres of *Xenopus laevis*. *Journal of Physiology* **151**, 491–501.

HEBERT, T. E., MONETTE, R., DUNN, R. J. & DRAPEAU, P. (1994). Voltage dependence of the fast and slow gating modes of RIIA sodium channels. *Proceedings of the Royal Society* B **256**, 253–261.

HILLE, B. (1992). *Ionic Channels of Excitable Membranes*, 2nd edn, pp. 21–58. Sinauer Associates Inc., Sunderland, MA, USA.

HODGKIN, A. L. & HUXLEY, A. F. (1952). A quantitative description of membrane current and its application to conduction and excitation in nerve. *Journal of Physiology* **117**, 500–544.

HORN, R. (1987). Statistical methods for model discrimination. Applications to gating kinetics and permeation of the acetylcholine receptor channel. *Biophysical Journal* **51**, 255–263.

HOWE, J. R. & RITCHIE, J. M. (1992). Multiple kinetic components of sodium channel inactivation in rabbit Schwann cells. *Journal of Physiology* **455**, 529–566.

HSU, H., HUANG, E., YANG, X., KARSCHIN, A., LABARCA, C., FIGL, A., HO, B., DAVIDSON, N. & LESTER, H. A. (1993). Slow and incomplete inactivation of voltage gated channels dominate encoding in synthetic neurons. *Biophysical Journal* **65**, 1196–1206.

ISOM, L. L., DE JONGH, K. S., REBER, B. F. X., OFFORD, J., CHARBONNEAU, H., WALSH, K., GOLDIN, A. L. & CATTERALL, W. A. (1992). Primary structure and functional expression of the $\beta 1$ subunit of the rat brain sodium channel. *Science* **256**, 839–842.

KEYNES, R. D. (1991). On the voltage dependence of inactivation in the sodium channel of the squid giant axon. *Proceedings of the Royal Society* B **243**, 47–53.

KEYNES, R. D. & ROJAS, E. (1976). The temporal and steady state relationships between activation of the sodium conductance and movement of the gating particles in the squid giant axon. *Journal of Physiology* **255**, 157–189.

KRAFTE, D. S., GOLDIN A. L., AULD, V. J., DUNN, R. J., DAVIDSON, N. & LESTER, H. A. (1990). Inactivation of cloned Na channels expressed in *Xenopus* oocytes. *Journal of General Physiology* **96**, 689–706.

LALIK, P. H., KRAFTE, D. S., VOLBERG, W. A. & CICCARELLI, R. B. (1993). Characterization of endogenous sodium channel gene expressed in Chinese hamster ovary cells. *American Journal of Physiology* **264**, C803–809.

NEUMCKE, B. & STÄMPFLI, R. (1982). Sodium currents and sodium-current fluctuations in rat myelinated nerve fibres. *Journal of Physiology* **329**, 163–184.

NUMANN, R., CATTERALL, W. A. & SCHEUER, T. (1991). Functional modulation of brain sodium channels by protein kinase C phosphorylation. *Science* **254**, 115–118.

OCHS, G., BROMM, B. & SCHWARZ, J. R. (1981). A three state model for inactivation of sodium permeability. *Biochimica et Biophysica Acta* **645**, 243–252.

PATLAK, J. (1991). Molecular kinetics of voltage dependent channels. *Physiological Reviews* **71**, 1047–1080.

RUBEN, P. C., STARKUS, J. G. & RAYNER, M. D. (1990). Holding potential affects the apparent voltage sensitivity of sodium channel activation in crayfish giant axon. *Biophysical Journal* **56**, 1169–1184.

SARKAR, S. N. & SIKDAR, S. K. (1994). High level stable expression of rat brain type IIA sodium channel α-subunit in CHO cells. *Current Science, India* **67**, 196–199.

SCHEUER, T., AULD, V. J., BOYD, S., OFFORD, J., DUNN, R. & CATTERALL, W. A. (1990). Functional expression of rat brain type IIA sodium channels expressed in a somatic cell line. *Science* **247**, 854–858.

STAFFAN, J. & ÅRHEM, P. (1992). Membrane currents in small cultured rat hippocampal neurons: a voltage clamp study. *Journal of Physiology* **445**, 141–156.

STARKUS, J. G., RAYNER, M. D., FLEIG, A. & RUBEN, P. C. (1993). Photodynamic modification by methylene blue: effects on fast and slow inactivation. *Biophysical Journal* **65**, 715–726.

STÜHMER, W., CONTI, F., SUZUKI, H., WANG, X., NODA, M., YAHAGI, M., KUBO, H. & NUMA, S. (1989). Structural parts involved in activation and inactivation of the sodium channel. *Nature* **339**, 597–603.

UKOMADU, C. & ZHOU, J. (1992). $\mu 1$ Na^+ channels expressed transiently in human embryonic kidney cells: biochemical and biophysical properties. *Neuron* **8**, 663–676.

VANDENBERG, C. A. & BEZANILLA, F. (1991). Single-channel, macroscopic, and gating currents from sodium channel in the squid giant axon. *Biophysical Journal* **60**, 1499–1510.

WEST, J. W., SCHEUER, T., MAECHLER, L. & CATTERALL, W. A. (1992). Efficient expression of rat brain type IIA Na^+ channel α subunits in a somatic cell line. *Neuron* **8**, 59–70.

Acknowledgements

Supported by grants from the Erna and Victor Hasselblad Foundation (Sweden) and the Department of Biotechnology, Government of India. S.N.S. was supported by a Senior Research Fellowship from the Council of Scientific and Industrial Research, India. Computations were done at the Supercomputer Education and Research Centre, Indian Institute of Science, Bangalore, India.

Received 14 November 1994; accepted 2 May 1995.